

SXD – the single-crystal diffractometer at the ISIS spallation neutron source

 David A. Keen,^{a*} Matthias J. Gutmann^a and Chick C. Wilson^b
^aISIS Facility, Rutherford Appleton Laboratory, Chilton, Didcot, Oxon OX11 0QX, UK, and

^bWestCHEM, Department of Chemistry, University of Glasgow, Glasgow G12 8QQ, UK.

Correspondence e-mail: d.a.keen@rl.ac.uk

Received 3 March 2006

Accepted 5 July 2006

 © 2006 International Union of Crystallography
 Printed in Great Britain – all rights reserved

SXD, the single-crystal diffractometer at the ISIS spallation neutron source, uses an array of two-dimensional position-sensitive detectors and the neutron time-of-flight technique to measure diffraction data throughout very large volumes of reciprocal space for each fixed orientation of a single-crystal sample. This paper describes SXD in detail, following major improvements to the instrument. Particular emphasis is placed on the range of science possible, using recent results as examples, and the opportunities for future experiments.

1. Introduction

The single-crystal diffractometer SXD (Wilson, 1990), at the ISIS Spallation Neutron Source (see <http://www.isis.rl.ac.uk>) at the CCLRC Rutherford Appleton Laboratory, has seen incremental improvements throughout its 18 years of existence. However, over the past five years, there has been a substantial upgrade to the instrumentation, which has significantly expanded its experimental capabilities. This, as described below, has come about as a result of a large increase in detector coverage, improved detector stability and an enhanced design that provides much better sample alignment and beam collimation.

The measurement method used on SXD has been described as a ‘time-sorted Laue’ technique (Turberfield, 1970). A polychromatic beam of neutrons is incident on a single-crystal sample and the scattered neutrons are collected in large-area position-sensitive detectors (PSDs) as a function of neutron time-of-flight (the time the neutron takes to reach the detectors from the spallation target, *via* the sample). In this manner, the orders of a given reflection are collected in the same detector pixel (similar to the Laue method), but each order is collected at a different neutron time-of-flight). The data from SXD therefore consist of a time-of-flight spectrum for each detector pixel. There is a linear relationship between neutron time-of-flight and wavelength and, for a given scattering angle 2θ and total flight path distance, neutron time-of-flight is proportional to crystal spacing, d (Ibberson *et al.*, 1992).

By way of an example, and noting that SXD uses area PSDs to measure diffraction data within volumes of reciprocal space, Fig. 1 shows how data within an area of reciprocal space are measured by a single-crystal diffractometer with a linear PSD covering scattering angles between $2\theta_{\min}$ and $2\theta_{\max}$ and collecting data between neutron time-of-flight_{min} and time-of-flight_{max}. The region covered corresponds to the portion of scattering from the sample incident on the detector enclosed by the two Ewald spheres of radii $2\pi/\lambda_{\max}$ and $2\pi/\lambda_{\min}$. The

number of Bragg reflections measured with one crystal position is therefore dependent on the source characteristics, the positioning of suitable detectors around the sample and the Bragg peak density for the given crystal sample. Maximizing the detector coverage has a number of advantages. First, collecting more Bragg reflections in each crystal orientation increases the speed of data collection. Secondly, fewer crystal

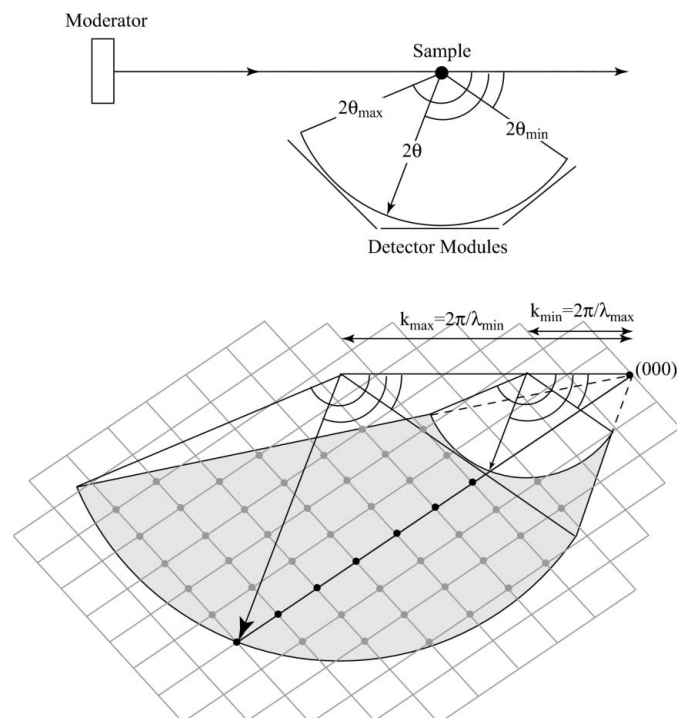


Figure 1 Diagram showing how the experimental arrangement for time-of-flight neutron single-crystal diffraction (top) corresponds to a measurement of a large region of reciprocal space (bottom). In addition, the lower figure shows how the orders of a given reflection appear at a fixed 2θ as a function of λ (bold line). (From Nield & Keen, 2001, after Turberfield, 1970.)

orientations are required to complete the full data collection. The net effect of both of these, provided that the instrument is designed to minimize the background and maintain a good signal-to-noise ratio, is that experiments using physically smaller samples or samples with larger, more complex structures may be attempted. Thirdly, since less crystal orientations are required, it is possible to simplify the crystal mounting and hence utilize more complicated sample environment equipment, such as high-pressure cells.

2. Instrument design

2.1. General layout of the diffractometer

The diffractometer is situated on beamline S3 of the 50 Hz first target station at ISIS. The instrument, with a primary flight path of 8.3 m, views the ambient temperature water moderator. Fig. 2 shows a photograph of the SXD diffractometer. It is designed to be compact and self-contained, with an integral detector and sample tank support frame. The rigidity of this frame, together with a careful survey of the

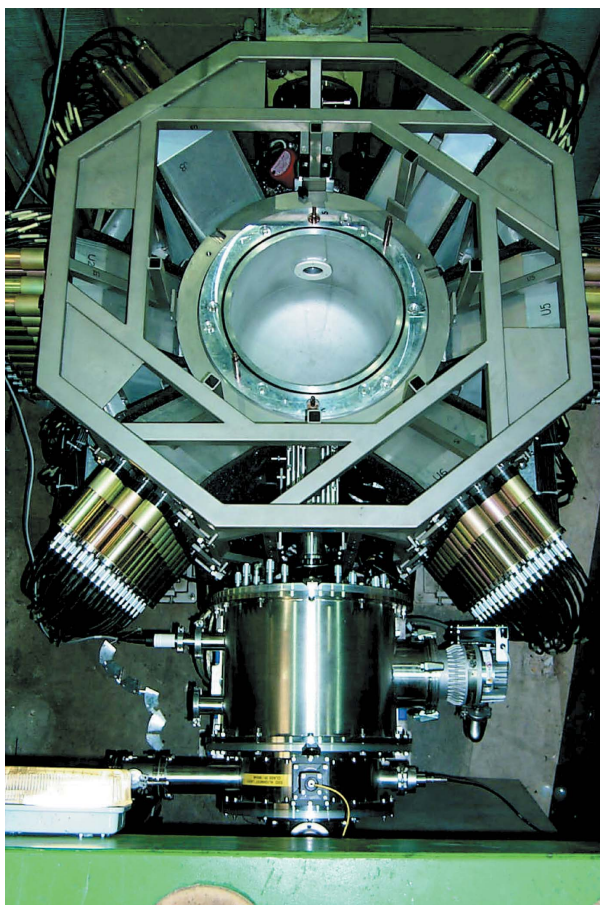


Figure 2
Photograph of SXD taken from above and with the incident neutrons from the ISIS target arriving from the bottom of this view. The octagonal frame supports the sample tank and surrounding detectors. The extra space in the top of the frame above detector 3 allows for off-vertical sample rotations (see text). The housings for the alignment laser and retractable mirror (bottom, nearest the shielding wall) and the pair of collimating jaws (large cylinder) can also be seen.

Table 1

Location of the eleven detectors on SXD.

Detector labels correspond to those indicated in Fig. 3; longitude, latitude and $L2$ are the scattering angle, angle out of the equatorial plane of the instrument and secondary flight path distance of the central pixel of each detector, respectively.

Detector	Longitude (°)	Latitude (°)	$L2$ (mm)
1	142.5	0.0	225
2	90.0	0.0	225
3	37.5	0.0	225
4	-37.5	0.0	225
5	-90.0	0.0	225
6	-142.5	0.0	225
7	90.0	-45.0	270
8	0.0	-45.0	270
9	-90.0	-45.0	270
10	180.0	-45.0	270
11	0.0	-90.0	280

instrument components into position during assembly, ensures a high degree of precision in terms of detector and sample location. This has been confirmed during later calibration of the diffractometer (see below). After removal of the shielding above the instrument, the whole detector and sample tank assembly may be lifted vertically as a single unit, fully cabled. This permits routine maintenance of the detectors, pumping equipment and other beamline components. In addition, this design makes it straightforward to move the diffractometer to a beamline with different characteristics in the future, if thought beneficial.

2.2. Detector array

The SXD instrument is designed to use as large an area of PSDs as possible in order to maximize the amount of scattering detected from the sample, whilst not impeding options for complex sample environment equipment. The detectors are placed in fixed positions as tabulated in Table 1. The flat front surface of each detector is aligned perpendicular to the vector joining the sample to the detector centre. Six detectors are in the equatorial plane, three on either side of the neutron beam, with a further five below the sample. Of these, four are at an angle of 45° to the equatorial plane and one is directly beneath the sample. Each detector consists of a square fibre-optically coupled scintillator PSD with 64×64 pixels, and an active area of 192×192 mm (*i.e.* each pixel is 3×3 mm). Details of the scintillator neutron detector system can be found elsewhere (Rhodes *et al.*, 1997). Fig. 3 shows the effective solid-angle coverage for the detector array. The front faces of the detectors are touching in the equatorial plane, at $2\theta \simeq 90^\circ$ and between the bottom detector and low- and high-angle detectors at 45° . In total, 49.4% of the scattering from the sample is collected by the detector array, largely in the lower half of the scattering sphere.

2.3. Sample support

The sample may be rotated about one of two possible axes. The first is an ω rotation about the vertical axis and the second is a φ rotation about a fixed $\omega = 45^\circ$, $\chi = 35^\circ$ axis (with respect

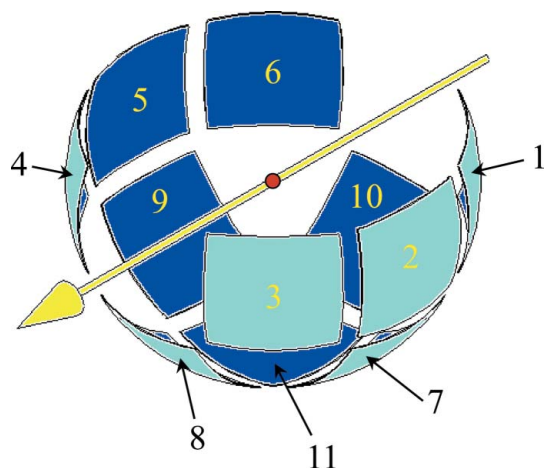


Figure 3
Figure showing the solid-angle coverage (represented by shaded regions on a sphere of fixed radius) corresponding to the detector arrangement on SXD.

to the transmitted beam and vertical axes, respectively). The former provides the best access for bulky sample environment items, whereas the latter gives good coverage of reciprocal space for complete data collections. In addition, the closed cycle helium refrigerator used on SXD has a further, internal, arc providing 45° rotation of the sample perpendicular to the φ axis. The sample is supported from above for ease of sample loading and to ensure that scattering from the sample to the detectors is not obscured by the sample mount. Two dowelled location pins are used to ensure reproducible placement of the sample rotation stage on the diffractometer.

2.4. Beamline components

Fig. 4 gives a schematic layout of the SXD beamline, showing the positions of the principal components. The beamline is designed to give a clean neutron beam with a maximum 12 mm diameter at the sample. This is achieved with a combination of collimation and shielding between the moderator and the sample. In particular, there are two sets of sintered boron carbide apertures at 990 mm and 755 mm before the sample position. These may be adjusted independently under computer control in both the horizontal and the vertical direction to give a full range of beam sizes at the sample position. There is also an optional boron nitride ‘beam scraper’ 196 mm before the sample position, the aperture of which can be changed manually to reduce the background from the beam penumbra. In addition, there is substantial shielding around all the beamline components and the minimum of vacuum windows in the beam to reduce the background levels in the detectors. This is extremely important since it is not possible to collimate the large PSDs effectively, especially since they are so close to the sample tank. Two pumps are used to

evacuate the beamline. The first provides a ‘rough’ vacuum in the ‘get-lost-pipe’ and the part of the beamline within the target shielding and around the incident-beam monitor. The second, placed close to the sample tank, produces a ‘cryogenic’ vacuum in the sample chamber sufficient for running ‘bare’ closed-cycle refrigerators or furnaces. The two windows separating these regions of the beamline are made of thin aluminium and are placed 1160 mm upstream and 690 mm downstream from the sample, respectively, far enough from the sample position that the scattering from them can be shielded effectively.

2.5. Sample alignment equipment

The instrument has facilities to enable accurate positioning of the sample on the centre of the rotation arcs and simultaneously in the centre of the neutron beam. These consist of a laser that is aligned along the path of the neutron beam *via* a retractable mirror (see Fig. 4) and equipment that replicates the geometry of the sample assembly off-line. The latter has two adjustable optical microscopes that view the sample from two directions perpendicular to each other and a distance gauge that can be used to check the precession of the sample rotation equipment. In addition, there are two setting jigs that can be attached to the sample rotation equipment for routine low-precision alignment of samples.

2.6. Sample environment equipment

The instrument can use all standard ISIS sample environment equipment, although some may not allow the whole SXD detector array to measure the scattering from the sample unimpeded. For this reason, SXD has a number of items of sample environment apparatus designed specifically for use on the diffractometer. These include a closed-cycle helium refrigerator, CCR (10 < T < 300 K), which may be used in conjunction with a 0.2 GPa or 0.5 GPa helium-gas pressure cell, and a helium cryostat (1.6 < T < 300 K). The CCR can be mounted on both axes mentioned above (see §2.3), but the cryostat can only be mounted on the vertical rotation axis. In addition, a dedicated high-temperature furnace will be available in the near future.

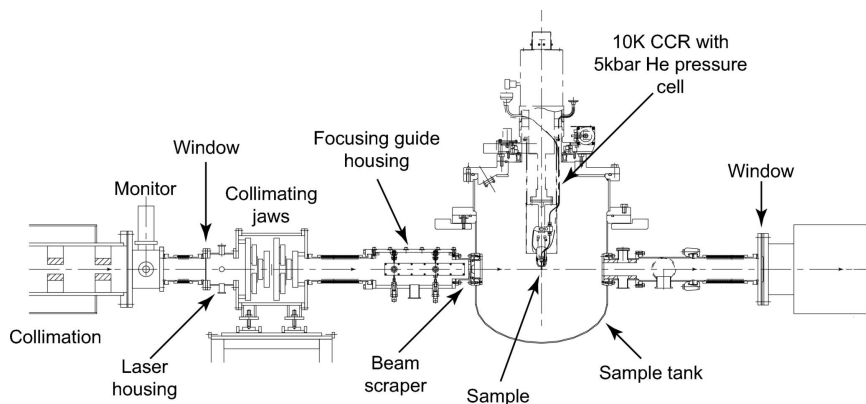


Figure 4
Drawing of the beamline components on SXD. The detectors are not shown for clarity; their arrangement is shown in Figs. 2 and 3.

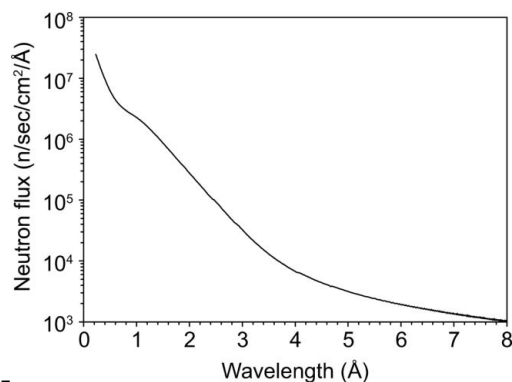


Figure 5
Neutron flux at the SXD sample position determined from measurements of a 'null scattering' V/Nb sphere.

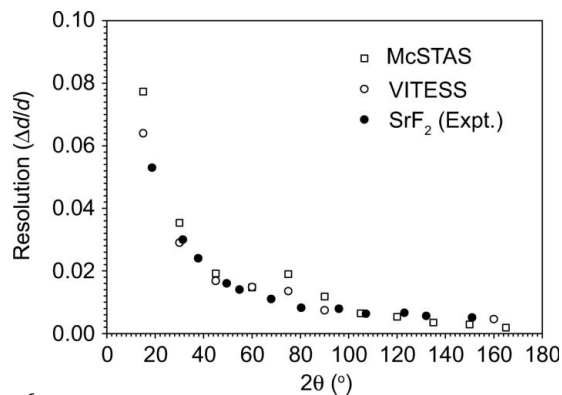


Figure 6
Neutron time-of-flight resolution (FWHM) of SXD in the equatorial plane as a function of scattering angle 2θ based on Monte Carlo simulations using *McSTAS* (Willendrup *et al.*, 2004; also see <http://neutron.risoe.dk/mcstas/>) and *VITESS* (see <http://www.hmi.de/projects/ess/vitess/>) codes and derived from measurements of a SrF_2 single crystal.

3. Instrument flux and resolution

The flux on SXD was determined from a 'null-scattering' $\text{V}_{0.946}\text{Nb}_{0.054}$ sphere of 3 mm radius (the composition is chosen to give zero coherent scattering from the sample). The flux shown in Fig. 5 is an average of the scattering from all eleven detectors after corrections for instrument background, sample absorption, detector efficiency (assumed to be 20% at 1 Å) and solid-angle coverage. The Maxwellian peak, which occurs at ~ 1 Å for the ISIS water moderator, is only seen as a weak shoulder to the strong high-energy epithermal region. It is likely that the change in slope at ~ 4 Å is a result of incomplete background subtraction rather than a real effect; the actual flux will fall more rapidly at high wavelengths. The integrated flux (for wavelengths between 0.2 and 8.7 Å) amounts to 6×10^6 neutrons $\text{cm}^{-2} \text{s}^{-1}$. The resolution in the equatorial plane of the instrument has been determined from measurements of Bragg peak widths from a small crystal of SrF_2 and compared with Monte Carlo simulations of the SXD instrument using *VITESS* (see <http://www.hmi.de/projects/ess/vitess/>) and *McSTAS* (Willendrup *et al.*, 2004; also see <http://neutron.risoe.dk/mcstas/>) as shown in Fig. 6. There is good consistency between what is observed experimentally and the simulation results. The best resolution is obtained in backscattering amounting to a time-of-flight pulse width of 0.5% $\Delta t/t$.

The accuracy of unit-cell parameters was assessed using a 6 mm diameter spherical sample of NaCl by taking twenty-one 11 min frames of data at different crystal settings. Each frame contained ~ 300 reflections yielding a refined cell parameter which was consistent within error (± 0.0035 Å) to the value from all the other frames. The average value determined was $a = 5.6332$ (8) Å, in good agreement with published values.

4. Instrument operation

4.1. Calibration

The instrument is aligned optically using the off-line alignment device to remove precession in the sample rotation, and using the instrument laser to ensure that the beam is coincident with the centre of rotation of the sample. The neutron beam is 'moved' by adjusting the collimating jaws. The laser spot can either be observed through optical apertures in the top flange of the sample tank, or through the read-out from a charge-coupled device (CCD) placed at the sample position. This procedure is not required before every experiment, and indeed for routine data collections, setting jigs that are attached to the sample rotation stage may be used to align the sample, albeit with lower precision. These jigs have been dowelled into position to point exactly at the centre of the rotation axis.

To calibrate the detector positions, the (pixel, time-of-flight) positions of the Bragg peaks from a sample with a known unit cell are used to refine the detector angles, sample to detector distances and offsets using the instrument software (see below). Further refinement of these values is usually also carried out for each experiment using the sample under study since they also depend on the characteristics of the sample and the accuracy of the positioning of the sample in the beam. Scattering from a V/Nb sphere is used to measure the incident neutron flux viewed by the detectors for subsequent data normalization. This scattering implicitly accounts for effects of detector pixel efficiency and solid angle.

4.2. Routine running

A typical measurement consists of mounting the sample (or samples, see §4.4) on the sample rotation stage (*e.g.* the cold finger of the CCR) using either the off-line alignment assembly or the sample setting jigs and checking the centering of the sample. The sample rotation stage is then mounted on the diffractometer. The beam-defining jaws are then adjusted to provide the required beam size, the instrument is evacuated and the neutron beam shutter opened. Data are accumulated for a number of frames using the standard ISIS instrument control program (Akeroyd *et al.*, 2002). Each frame consists of a single exposure of the sample to the neutron beam for a fixed amount of time (or integrated beam current) whilst the sample is stationary. The amount of time for each frame depends on the crystal size and structural complexity, but would be typically between 30 min and 6 h. The sample is then rotated by a given amount and re-exposed. A complete data collection may only require a small number of frames. This is then repeated

for each temperature or pressure point of interest. Additional runs may be required to characterize the background or incident flux for data normalization to complete the measurement.

4.3. Data-reduction software

The instrument's user-friendly software, *SXD2001*, allows the experimenter to extract normalized Bragg intensities or corrected diffuse scattering data from SXD measurements. The graphical user interface (see Fig. 7) to the program uses the IDL graphical display package (see <http://www.itervis.com/idl/>). The sequence for data treatment is as follows.

(i) Each frame of data is searched to identify the positions of possible Bragg peaks, given in terms of an (x, z, t, n) coordinate, where x and z identify the horizontal and vertical positions of the pixel of detector n containing the possible peak at time-of-flight t .

(ii) Trial **UB** matrices (Busing & Levy, 1967; Keen & Wilson, 1996) are then generated until one is found to account for some or all of the possible peak positions based on the known or expected crystal unit cell. More than one **UB** matrix may be used if more than one single crystal is exposed to the neutron beam.

(iii) These **UB** matrices, cell constants and other instrument parameters are then refined using a complete set of identified Bragg peak positions to optimize the match between observed and calculated peak positions.

(iv) (a) The peak intensities are determined, based on either the observed or the calculated peak positions, using a peak fitting routine which uses the characteristic peak line shape as a function of neutron time-of-flight. (b) Alternatively, the data are normalized following procedures routinely used for total scattering (e.g. Howe *et al.*, 1989) and extracted as a volume of reciprocal space for diffuse scattering visualization or fitting.

4.4. Multi-crystal data collection

The multi-crystal method has been developed on SXD (Wilson, 1997) and used extensively (see experiments described in §5), since it is the ideal instrument for such methods. The principle is straightforward and has been used inadvertently (during single-crystal diffraction experiments on samples which are not 'single') in the past (for example, Gao *et al.*, 1994). A small number of crystals (up to six, but three is more typical) of the same compound are placed in the neutron beam in different orientations and measured as described above (§4.2). The time-sorted Laue method used on SXD means that the detectors collect the Bragg reflections from each crystal simultaneously and the majority of Bragg reflections from the different crystals do not overlap each other. The instrument software can then be used to extract the Bragg intensities from the different crystals, discarding the reflections that are found to overlap. As a result, a complete data set may be collected significantly more quickly (in proportion to the number of crystals exposed), or with significantly greater over-determination of Bragg peak intensities, or from experimental arrangements with reduced flexibility (pressure cells, smaller scattering apertures *etc.*).

5. Example experiments

Here a number of recent experiments on SXD are outlined, chosen to demonstrate the instrument's characteristics and versatility. The majority of experiments on SXD use the instrument to locate hydrogen atoms in crystalline materials to augment existing X-ray diffraction crystal structure determination. This is an established strength of single-crystal neutron diffraction (Wilson, 2000) and is used for studies of all aspects of hydrogen-bonding and charge-density studies. However, a growing area of work on SXD concerns parametric studies of molecular systems, either as a function of temperature or pressure, where the characteristics of SXD, coupled with the multi-crystal method, CCRs and/or helium gas pressure cells, are ideally suited to such measurements.

5.1. Structure determination of L- and D-alanine

In the search for observations of the physico-chemical basis for chiral selection in macromolecules, a number of experiments have been reported that claim to detect some indication of such a parity violating phase transition in amino acids. Recently, these experimental results, from differential scanning calorimetry, magnetic susceptibility and Raman spectroscopy, have been seriously questioned. X-ray diffraction measurements of a series of amino acids appear to show no

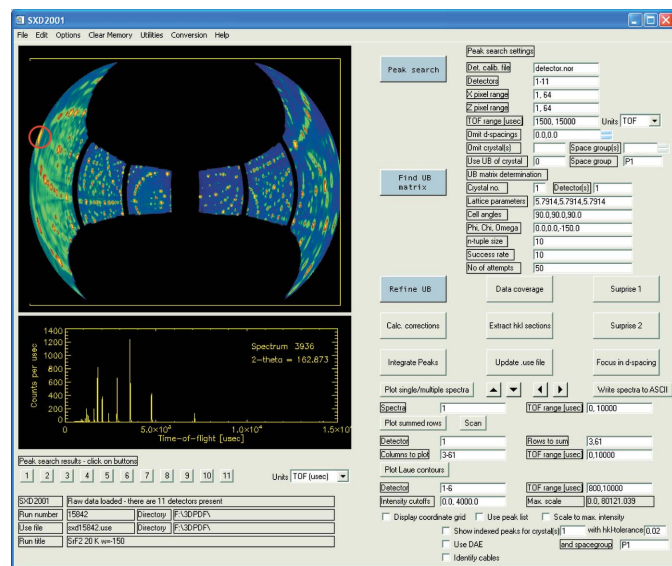


Figure 7 Screen capture of the *SXD2001* data-reduction graphical user interface. The top left-hand panel shows a time-integrated representation of the scattering collected by the six equatorial detectors looking from the moderator along the neutron beam, and clearly showing the Laue-like nature of the data collection. The bottom left-hand panel shows the scattering in one detector pixel as a function of neutron time-of-flight and with the orders of a Bragg reflection separated in time-of-flight. The pixel being displayed corresponds to the circled bright spot at the far left of the Laue plot above (*i.e.* at the high-angle edge of high-angle detector 1). The data are from a sample of SrF₂, measured on SXD at 20 K.

convincing evidence for any associated structural effect. In order to eliminate the possible role of subtle hydrogen-atom effects in this supposed transition conclusively, an accurate single-crystal neutron diffraction study of the amino acid alanine was carried out on SXD, on both enantiomers, above and below the putative phase-transition temperature (Wilson *et al.*, 2005).

The SXD experiment is a good example of the type of systematic accurate study made feasible by the upgraded instrument. Data were collected from large single crystals of both D- and L-alanine (crystal volumes $\sim 5\text{--}10\text{ mm}^3$), at 295 and 60 K, with good redundancy to sufficient $\sin\theta/\lambda$ resolution to allow accurate determination of hydrogen-atom positions and vibrational parameters. Although carried out at a time when only six of the eleven PSDs were operational, the total data collection time for the full study was around four to five days of SXD time. The refined structures are shown in Fig. 8; the refined parameters, when corrected for routine thermal motion effects, show no significant differences in any of the measured structures. This result showed conclusively that there is no observable structural change in this material and calls into question the existence of the postulated phase transition.

5.2. Multi-crystal structure determination: acetylcholine bromide

SXD structural studies of the neurotransmitter molecule acetylcholine were carried out in order to elucidate its hydrogen-bonding interactions, along with other non-bonded interactions involving hydrogen atoms. In the original 'routine' SXD study at 100 K (Shankland *et al.*, 1997), a pattern of interesting contacts of the methyl hydrogen atoms

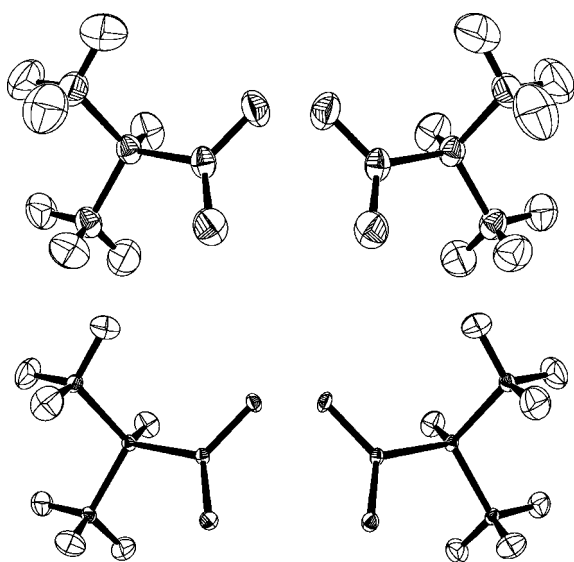


Figure 8

The structures of L- and D-alanine determined by neutron diffraction on SXD at 295 K and 60 K: (top left) L-alanine at 295 K, (top right) D-alanine at 295 K, (bottom left) L-alanine at 60 K, (bottom right) D-alanine at 60 K.

(deuteriums) with the bromide ions was determined. This material was then used as a demonstration molecule for the development of the multi-crystal method (see §4.4) (Wilson, 1997).

The single crystals of acetylcholine bromide ($\text{C}_7\text{D}_{16}\text{O}_2\text{N}^+\text{Br}^-$) used in this experiment were cut from a large sample on which the original 100 K SXD experiment had been carried out. The sample was fully deuterated and thus has a lower incoherent neutron scattering background than for a hydrogenous sample, making it particularly appropriate for what was the first test of the multi-crystal procedure on SXD. The samples used were of approximate dimensions 1.5, 3 and 3 mm^3 . The data were collected from the sample with all three crystals exposed to the beam, mounted along a vertical axis, in a series of ω steps. The exposure time for each frame was approximately 2 h, with the entire data set collected in approximately 10–12 h, with a good level of redundancy.

The resulting model is shown in Fig. 9, from which it can be seen that a good quality structural refinement has been achieved from the multi-crystal sample. Most importantly, it is evident that full three-dimensional information has been made available from a simple ω rotation of the sample. This is evident both in the very satisfactory definition of the thermal ellipsoids of all atoms, but also in the fact that the absolute estimated standard uncertainties are roughly equal in all directions. Clearly, the restricted geometry of the data collection has been overcome by the quasi-random design of the multi-crystal sample. The structural parameters obtained show good agreement with previous determinations.

5.3. Rapid variable-temperature studies: proton migration in urea phosphoric acid

The accurate determination of hydrogen-atom positional and anisotropic displacement parameters, ideally studied by neutron diffraction, can often reveal much of interest even in apparently 'normal' crystal structures. The structure of urea phosphoric acid shows just such interesting hydrogen-atom behaviour. The focus here is on the hydrogen atom in the short

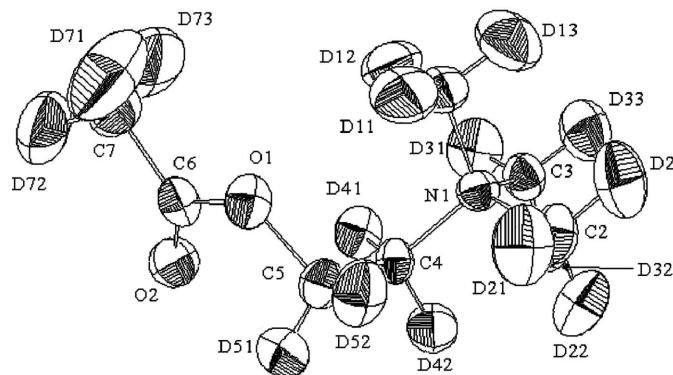


Figure 9

The structure of the (deuterated) acetylcholine molecule as refined from multi-crystal data collected on SXD from the bromide salt at room temperature.

strong O—H···O hydrogen bond linking the two moieties in the complex (O···O distance ~ 2.41 Å).

There is great current interest in such short strong hydrogen bonds, both in the chemical and the biological fields. In contrast to ‘normal’ and weak, very strong hydrogen bonds have a quasi-covalent character in which the hydrogen atom is involved in two partial covalent bonds of comparable bond orders, and the potential energy profile defining such a hydrogen bond is usually best described as a broad single well. This study was carried out on SXD at an unprecedentedly large number of temperature steps using the multi-crystal technique (Wilson, 2001), and supported by conventional variable-temperature single-crystal measurements (Wilson *et al.*, 2001). The multi-crystal SXD experiment allowed neutron diffraction studies of the structure to be undertaken between 150 K and 350 K, with determinations between 280 and 335 K in very fine temperature steps of 5–10 K. The conventional determination was carried out at seven temperatures between 150 and 350 K. A total of 19 snapshots were obtained in five to six days, allowing a robust determination of the behaviour of the proton.

The most striking finding in the experiment is the systematic increase in the $O_{\text{urea}}\cdots H$ distance with increasing tempera-

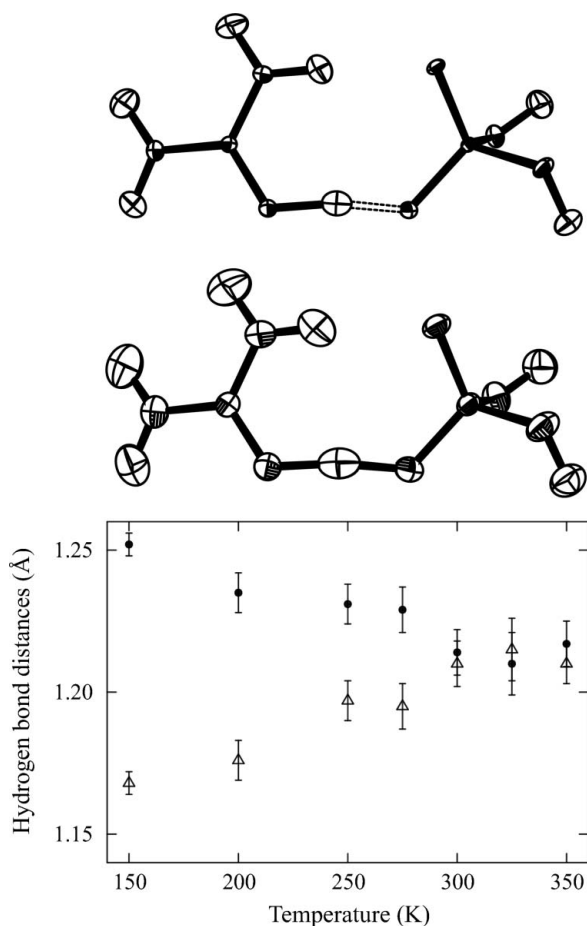


Figure 10 (Top) Views of the structure of urea-phosphoric acid at 150 K (upper picture) and 350 K (lower picture), and (bottom) a plot of the tendency of the two O—H separations to become equal with increasing temperature: the proton migrates to the centre of the hydrogen bond.

ture, and the corresponding tendency of the hydrogen bond to become more symmetric (Fig. 10). Thus, with increasing temperature, this hydrogen atom migrates towards the midpoint of the hydrogen bond. This shift in position of the hydrogen atom with temperature (by up to ~ 0.04 Å) implies that the position of the broad single well potential minimum also shifts slightly with temperature. Such a shift might arise as a consequence of the effect of crystal packing due to changes in the local environment with temperature and the results have encouraged substantial theoretical modelling (Morrison *et al.*, 2005; Fontaine-Vive *et al.*, 2006).

5.4. A high-pressure study of potassium hydrogen maleate

The hydrogenmaleate ion contains a short strong hydrogen bond where the position of the hydrogen atom is sensitive to the crystallographic environment. Prior to this SXD experiment, neutron diffraction studies had confirmed the centring of this proton, located on a mirror plane, in the potassium salt at a range of temperatures. The experiments carried out on SXD were aimed at investigating the possible effect of pressure on this symmetric hydrogen bond.

The high-pressure cell used in this study is constructed of TiZr ‘null’ scattering alloy (the proportions of the two elements are again chosen so as to give zero overall coherent neutron scattering length). The cell is based on a similar device used on the SCD instrument at IPNS, Argonne, but redesigned to allow applied pressures of up to 0.5 GPa using He gas provided by an off-line intensifier. The cell can also be mounted on a CCR, for simultaneous cooling to ~ 30 K. From a practical point of view, the mounting of the cell is restricted to a vertical geometry and in order to obtain representative three-dimensional single-crystal diffraction data, a multi-crystal sample is routinely used with this device.

Neutron diffraction data were collected on SXD under eight sets of thermodynamic conditions in the range 30–295 K and 0–0.4 GPa, with data collection times as low as 5 h per (p, T) point (Wilson *et al.*, 2003). These measurements, yielding good coverage of p – T space, allowed fully anisotropic refinements to be carried out on all data sets. The results of these refinements are shown in Fig. 11; these show the intramolecular hydrogen bonding in the structure to be essentially invariant in the range of conditions studied. Although a ‘null’ result, this work has shown that it is possible to carry out systematic investigations into the effects of variable temperature and variable pressure on molecular systems using single-crystal neutron diffraction.

5.5. Magnetic structure of $TbMn_2O_5$

Studying magnetic ordering is an emerging theme on time-of-flight Laue diffractometers, although it is not yet carried out routinely. Nevertheless, examples are now emerging which take advantage of the ability to collect fairly complete data in a relatively short time and to identify unknown magnetic propagation vectors from measured volumes of reciprocal space. $TbMn_2O_5$ is a multiferroic manganite where magnetic and electric properties are coupled. The commensurate

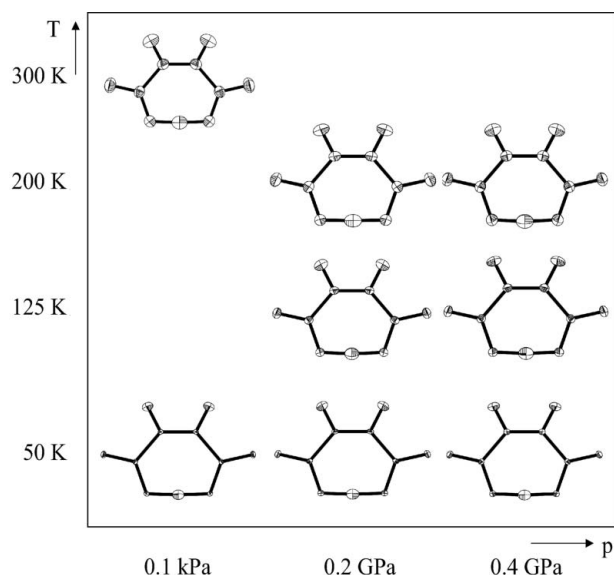


Figure 11
‘Structural phase diagram’ showing the refined structure of the hydrogenmaleate anion in potassium hydrogen maleate, from single-crystal neutron diffraction data collected on SXD at a range of temperatures and pressures.

magnetic phase was studied at 27 K (Chapon *et al.*, 2004). The challenge in this particular case was that there are a total of 12 magnetic ions in the unit cell, four Tb^{3+} , four Mn^{4+} and four Mn^{3+} , each of which can support its own independent spin wave. As a result, the number of possible models were not reduced sufficiently by symmetry analysis. Therefore, a simulated annealing approach was used to solve the magnetic structure. The resulting structure showed that the moments were confined to the (a, b) plane pointing predominantly along \mathbf{a} with a small canting angle. Simple phase relationships were found between the magnetic moments on the different sublattices. The moment on Tb was found to be induced by Mn ordering. An analysis of the resulting structure in terms of nearest-neighbour exchange paths revealed the system to be highly frustrated.

5.6. Diffuse scattering in benzil

SXD is particularly suited to diffuse scattering studies where diffuse features are often widely spread in regions of reciprocal space that are often not known beforehand. The diffuse scattering in a deuterated single crystal of benzil, $\text{C}_{14}\text{D}_{10}\text{O}_2$, was studied at room temperature (Welberry *et al.*, 2003) (see Fig. 12). The molecule is made up of two phenyl rings linked by an O–C–C–O bridge. An *ab initio* molecular dynamics calculation predicted the two phenyl rings to undergo torsional motion around the O–C–C–O bridge with an energy of about 3.1 meV. Inelastic effects from this torsional motion were evidenced in the appearance of the diffuse scattering around the 004 and 002 reflections when measured in different detectors and hence at different incident neutron energy. In particular, the splitting of the diffuse line around 004 allowed the energy of the phonon mode to be estimated to 1.1 meV.

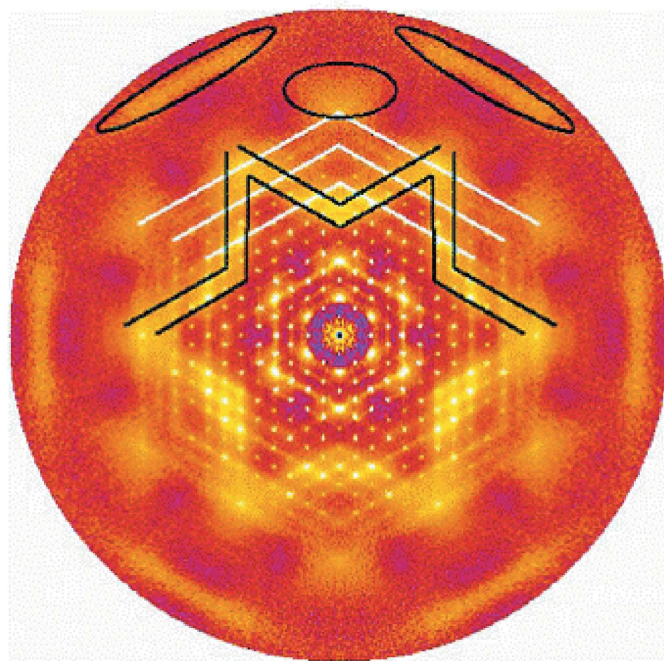


Figure 12
Diffuse neutron scattering from a deuterated single crystal of benzil in the $(hk0)$ reciprocal-lattice plane. The plot shows data measured using neutron energies greater than ~ 27 meV and from the equatorial detectors on SXD. Dark lines identify broad regions of diffuse intensity and white lines emphasize narrow lines of scattering.

6. Conclusions and further developments

This paper has described the general purpose single-crystal diffractometer, SXD, at the ISIS spallation neutron source, following substantial improvements to its design, instrumentation, operation and software. The diffractometer provides excellent instrumentation for a wide range of scientific applications, including parametric structural studies as a function of pressure and/or temperature, large scale reciprocal-space surveys and identification of unknown magnetic or structural propagation vectors.

Fig. 5 shows that the neutron flux incident on a sample on SXD is dominated by neutrons of short wavelength ($\lambda < 2$ Å). Although this is ideal for high-resolution studies and diffuse scattering measurements to high Q , it is less appropriate for magnetic studies, or other investigations which also require good information at low Q and/or long d -spacings. For this reason, a compact focusing device is being designed and tested for SXD. This device (Keen *et al.*, 2006) will significantly enhance the long-wavelength flux on SXD, perhaps by a factor of around 20 for wavelengths above 4 Å and small samples, and provide a more balanced flux distribution on the sample. Furthermore, the instrument design makes it relatively straightforward to move the diffractometer to a beamline with a different flux profile. The possibility of moving the instrument to a beamline which views a methane moderator, with a larger long-wavelength flux, can also be envisaged.

SXD has the largest detector coverage and the highest integrated neutron flux of any instrument of its type worldwide and it, together with SCD (Schultz, 1993; see <http://>

www.pns.anl.gov/instruments/scd/) at IPNS, Argonne, is a benchmark for all single-crystal time-of-flight neutron diffractometers under construction or being designed. The fact that the range of single-crystal diffractometers at spallation neutron sources is expanding [e.g. towards protein (Langan *et al.*, 2004; Schultz *et al.*, 2005) and other large-molecule crystallography] further emphasizes the success of the current SXD instrumentation.

We are grateful to EPSRC for providing the funding for the building and commissioning of SXD, to D. J. McPhail for designing the instrument, to the SXD Working Group and to the many scientists who have supported this instrument, especially those who have allowed us to use their results in this paper.

References

- Akeroyd, F. A., Campbell, S. I. & Moreton-Smith, C. M. (2002). <http://www.arXiv.org/cond-mat/0210468>.
- Busing, W. R. & Levy, H. A. (1967). *Acta Cryst.* **22**, 457–464.
- Chapon, L. C., Blake, G. R., Gutmann, M. J., Park, S., Hur, N., Radaelli, P. G. & Cheong, S. W. (2004). *Phys. Rev. Lett.* **93**, 177402.
- Fontaine-Vive, F., Johnson, M. R., Kearley, G. J., Howard, J. A. K. & Parker, S. F. (2006). *J. Am. Chem. Soc.* **128**, 2963–2969.
- Gao, Q., Weber, H.-P., Craven, B. M. & McMullan, R. K. (1994). *Acta Cryst.* **B50**, 695–703.
- Howe, M. A., McGreevy, R. L. & Howells, W. S. (1989). *J. Phys. Condens. Matt.* **1**, 3433–3451.
- Keen, D. A., Dalglish, R. M., Gutmann, M. J. & Webster, J. R. P. (2006). *Physica B*. In the press.
- Keen, D. A. & Wilson, C. C. (1996). Rutherford Appleton Laboratory Report, RAL-TR-96-083.
- Ibberson, R. M., David, W. I. F. & Knight, K. S. (1992). Rutherford Appleton Laboratory Report, RAL-92-031.
- Langan, P., Greene, G. & Schoenborn, B. P. (2004). *J. Appl. Cryst.* **37**, 24–31.
- Morrison, C. A., Siddick, M. M., Camp, P. J. & Wilson, C. C. (2005). *J. Am. Chem. Soc.* **127**, 4042–4048.
- Nield, V. M. & Keen, D. A. (2001). *Diffuse Neutron Scattering from Crystalline Materials*. Oxford University Press.
- Rhodes, N. J., Wardle, A. G., Boram, A. J. & Johnson, M. W. (1997). *Nucl. Inst. Methods A*, **392**, 315–318.
- Schultz, A. J. (1993). *Trans. Am. Crystallogr. Assoc.* **29**, 29–41.
- Schultz, A. J., Thiyagarajan, P., Hodges, J. P., Rehm, C., Myles, D. A. A., Langan, P. & Mesecar, A. D. (2005). *J. Appl. Cryst.* **38**, 964–974.
- Shankland, N., Florence, A. J. & Wilson, C. C. (1997). *Acta Cryst.* **B53**, 176–180.
- Turberfield, K. C. (1970). *Thermal Neutron Diffraction*, edited by B. T. M. Willis, p. 34. Oxford University Press.
- Willendrup, P., Farhi, E. & Lefmann, K. (2004). *Physica B*, **350**, E735–E737.
- Wilson, C. C. (1990). *IOP Conf. Ser.* **107**, 145–163.
- Wilson, C. C. (1997). *J. Appl. Cryst.* **30**, 184–189.
- Wilson, C. C. (2000). *Single Crystal Neutron Diffraction from Molecular Materials*. Singapore: World Scientific.
- Wilson, C. C. (2001). *Acta Cryst.* **B57**, 435–439.
- Wilson, C. C., Myles, D. A. A., Ghosh, M., Johnson, L. N. & Wang, W. (2005). *New J. Chem.* **29**, 1318–1322.
- Wilson, C. C., Shankland, K. & Shankland, N. (2001). *Z. Kristallogr.* **216**, 303–306.
- Wilson, C. C., Thomas, L. H. & Morrison, C. A. (2003). *Chem. Phys. Lett.* **381**, 102–108.
- Welberry, T. R., Goossens, D. J., David, W. I. F., Gutmann, M. J., Bull, M. J. & Heerdegen, A. P. (2003). *J. Appl. Cryst.* **36**, 1440–1447.